Version of Record: https://www.sciencedirect.com/science/article/pii/S0031018218301482
Manuscript_7d21bbc1898eb41068c96a1cccc65540

Paleogeographic differences in temperature, water depth and conodont biofacies during the Late Devonian

Girard, Catherine[1, *], Cornée, Jean-Jacques[2, 3], Joachimski, Michael M.[4], Charruault, Anne-Lise[1], Dufour, Anne-Béatrice[5], Renaud, Sabrina[5]

[1] Institut des Sciences de l'Evolution, Université de Montpellier, UMR5554 CNRS, IRD, EPHE, Place Eugène Bataillon, CC65, 34095 Montpellier cedex, France (catherine.girard@umontpellier.fr; anne-lise.charruault@umontpellier.fr)
[2] Géosciences Montpellier, Université de Montpellier, 34095 Montpellier Cedex 05, France (jean-jacques.cornee@gm.univ-montp2.fr)
[3] current address : Université des Antilles, Campus de Fouillole, 97170 Pointe-à-Pitre, France
[4] GeoZentrum Nordbayern, University of Erlangen-Nuremberg, Schlossgarten 5, D-91054 Erlangen, Germany (michael.joachimski@fau.de)
[5] Laboratoire de Biométrie et Biologie Evolutive, UMR 5558, Université de Lyon, Université Lyon 1, CNRS, 69100 Villeurbanne, France (sabrina.renaud@univ-lyon1.fr; anne-beatrice.dufour@univ-lyon1.fr)

*corresponding author

Abstract

The Famennian (Late Devonian) started after and ended with two of the seven largest crises of the Phanerozoic, the Kellwasser and Hangenberg events, respectively. In between, global environmental trends have been identified, involving cooling and eustatic regression. Tropical and subtropical marine faunas were largely cosmopolitan. Overall, this suggests that the Famennian was marked by long-term environmental changes occurring in a relatively homogeneous manner despite being punctuated by several short-term events of limited faunal impact. How these trends were modulated according to geographic location is investigated in this study by comparing two continuous outcrops in the Montagne Noire (Col des Tribes section, France) and in Saxo-Thuringia (Buschteich section, Germany). Both were located in the subtropical area during this period and belonged to two former microcontinents bracketed between the closing Rheic Ocean and Gondwana. Sedimentary facies, oxygen isotopes, and the generic conodont composition (biofacies) were studied in a high resolution and in the same rock samples. Sedimentary facies provided an estimate of water depth and oxygen

© 2018 published by Elsevier. This manuscript is made available under the CC BY NC user license
https://creativecommons.org/licenses/by-nc/4.0/

isotopes were used as paleotemperature proxy. Conodont biofacies were analyzed using a principal component analysis, allowing the expression of the variations in the two outcrops on the same axes, and a quantitative comparison with the other proxies. Sea-level and temperature variations were different between the two areas. Saxo-Thuringia displayed stable deep and warm conditions throughout. In contrast, the environment of the Montagne Noire was shallower and cooler during the Late and latest Famennian compared to the Early and Middle Famennian, congruent with the global change evidenced elsewhere. The location of Saxo-Thuringia, close to the first point of closure of the Rheic Ocean, might have favored active tectonics, causing a local departure from the eustatic trend. The stable temperatures at BU during the Late and latest Famennian may be due to the position of Saxo-Thuringia in the remnant Rheic Ocean, limiting water mass exchange with open seas, and favoring the persistence of warm conditions. Offshore taxa persisted later at high abundance in the Saxo-Thuringian record. The two conodont biofacies records were otherwise very comparable. This suggests that other factors mitigated the water depth forcing on these conodont assemblages.

Keywords. Famennian; Montagne Noire; Saxo-Thuringia; *Palmatolepis*; oxygen isotopes; sedimentary facies

1. Introduction

The Famennian is well known for being bracketed by two of the most important biological crises in the Earth's history: the Upper Kellwasser Event just before the Frasnian-Famennian boundary (e.g. McGhee, 1996; Schindler, 1993; Walliser, 1996) and the Hangenberg Crisis punctuating the Devonian-Carboniferous boundary (e.g. Becker et al. 2016; Kaiser et al. 2008, 2015; Walliser, 1996). Many studies were devoted to these crises, allowing a fine-scale characterization of the biotic and abiotic variations during the hundred thousand years involved in these worldwide perturbations (Becker et al., 2012; Corradini, 2003; Girard and Feist, 1997; Joachimski et al., 2009; McGhee, 1996; Sandberg et al., 1988; Walliser, 1996). Environmental changes also occurred during the time interval between the crises (ca. 13 Myr, Becker et al., 2012), but deserved much

less attention. Short-term events have nevertheless been described, with minor impact on the faunas (e.g. *Annulata* Events by House, 1985; Korn, 2004; Hartenfels, 2011; Hartenfels and Becker, 2017; Dasberg Crisis by Becker, 1993; Hartenfels and Becker, 2009; Hartenfels, 2011; Condroz Events by Becker, 1993; Becker and House, 1997). A regressive trend punctuated by minor transgressive-regressive couplets has been evidenced for the Famennian (Johnson et al., 1985, 1996). Global cooling inferred from oxygen isotope data has been suggested for the same interval (Joachimski et al., 2004, 2009), an interpretation supported by independent evidence of Latest Famennian glacial deposits described from South America (Caputo et al., 2008; Isaacson et al., 2008). The congruence of climate cooling and a regressive trend is therefore coherent in this eustatic context. Tropical and subtropical marine faunas were cosmopolitan at the generic level (Feist and Becker, 1997; Korn and De Baets, 2015; Mottequin et al., 2013; Spalletta et al., 2017) suggesting rather homogeneous environmental conditions and efficient exchanges between the faunas. Conodonts, small, nektonic animals of chordate affinities, were an abundant part of this marine fauna. Their taxonomic identification provides a detailed stratigraphic framework for this period (Hartenfels, 2011; Spalletta et al., 2017; Ziegler, 1962; Ziegler and Sandberg, 1984; 1990). Conodonts can also give paleoenvironmental indications because conodont genera distribution was influenced by several factors (Lüddecke et al., 2017), notably water depth (Sandberg, 1976; Seddon and Sweet, 1971). The congruence of temporal variations in the conodont biofacies (i.e. assemblage composition of the different genera) in different sections supported that the Famennian was marked by long-term environmental changes that were not durably perturbed by the short-term events punctuating it (Corradini, 2003; Girard et al., 2014; 2017).

This view, however, can also be the consequence of the paucity of detailed records in different paleogeographic areas. Famennian paleogeography was characterized by the closure of the Rheic Ocean bracketing microcontinents derived from Gondwana (e.g. Franke et al., 2017; Stampfli et al., 2013) (Fig. 1). Discrepancies in relative sea-level changes have been reported from these microcontinents (e.g. in the Saxo-Thuringian area) and attributed to tectonic movements overprinting the global eustatic trend (Girard et al., 2017). This raises the question whether the environmental trends evidenced so far are of global significance, and/or whether local/regional factors

related to tectonics and paleogeographic changes interfered with these (presumed) global trends.

To address these questions, we studied two recently described sections having a detailed record from the Late Frasnian to the end-Famennian (Girard et al., 2014, 2017). The Col des Tribes (CT) section in the Montagne Noire was part of the Armorica microcontinent, whereas the Buschteich section (BU) was located on the Saxo-Thuringian microplate. Hence, both sections were located on former microcontinents bracketed between the closing Rheic Ocean and Gondwana (Fig. 1). Water depth and approximate position relative to the shore were assessed based on the macroscopic description of the sediments as well as microfacies analysis (e. g. Flügel, 2004). Despite limitations due to the scarcity of preserved bioclasts in the sediments (e.g. Brett and Allison, 1998), this approach provided a paleoenvironmental estimate directly based on the depositional environment. Water depths derived from sedimentological analysis were compared with conodont biofacies, which have been proposed to react more sensitive to water-depth changes than microfacies (Lüddecke et al., 2017). Nevertheless, as for any biotic record, evolutionary changes through time (changes in water depth preferences, decrease or increase in response to biotic factors such as predation or competition) may interfere with the paleoenvironmental signature (Belka and Wendt, 1992). A multivariate approach was developed to quantitatively compare the conodont assemblages in the studied sections. In addition, paleotemperatures were reconstructed using oxygen isotopes measured on conodont apatite.

A strength of this study is that the three proxies are derived from the same rock samples taken at a comparable temporal resolution, allowing for detailed and quantitative comparisons. The following questions are addressed: (1) Did environmental changes affect similarly and at the same pace both areas, and if not, how to interpret any discrepancies? (2) Did water depth and temperature covary, as expected for eustatic trends during a global cooling culminating with the Devonian-Carboniferous boundary glaciation (Buggisch et al. 2008; Caputo et al., 2008; Isaacson et al., 2008)? (3) Was the forcing of water depth changes recorded as expected on conodont biofacies? In that context, did conodont biofacies rather react to local deviations from, or to globally recorded paleoenvironmental trends?

2. Geological setting

During the Late Devonian, the Col des Tribes (CT; Montagne Noire/France; Girard et al., 2014) and Buschteich (BU; Thuringia/Germany; Girard et al., 2017) sections were located in subtropical latitudes on different microcontinents (Fig. 1). These microcontinents progressively migrated towards the equator and Laurussia during this period due to the closure of the Rheic Ocean (Franke et al., 2017). The absence of provincialism in benthic faunas compared to Laurussian faunas suggests that the Rheic Ocean was, at that time, already reduced (Feist and Becker, 1997; Mottequin et al., 2013). It has been proposed that the Saxo-Thuringia microcontinent, on which BU was located, was situated in the middle of the sea between the remnant Rheic Ocean and the Paleotethys (Franke et al., 2017) during the Late Frasnian (375 Ma). By the latest Famennian (~360 Ma), this seaway was almost or completely closed, locating BU at the margin of the remnant Rheic Ocean (Fig. 1). The Montagne Noire, including CT, was located on the Armorica microcontinent which was presumably positioned further towards the Paleotethys Ocean. Nevertheless, the precise location of these microcontinents relative to Laurussia as well as their position relative to each other is debated (e.g. Eckelmann et al. 2014; Franke et al. 2017).

Both sections expose Late Frasnian to Late Famennian deposits, although with a gap during the earliest Famennian in BU. Their stratigraphical context has been formerly described (Girard et al., 2014, 2017) using the zonation of Ziegler and Sandberg (1990); and has been updated applying the zonation of Spalletta et al. (2017) in this study (Fig. 2). The CT section (Girard et al., 2014) is ca. 80 m thick. It consists of fine-grained bioclastic limestones from the *Palmatolepis rhenana* to the *Pa. glabra pectinata* conodont Zone, followed by typical reddish griottes from the *Pa. rhomboida* to the *Pa. marginifera marginifera* Zone. Lime mudstones were deposited from the *Pa. marginifera utahensis* to the *Pa. rugosa trachytera* Zone and are overlain by wackestones with an age from the *Polygnathus styriacus* to the middle of the *Bispathodus ultimus* Zone. The Famennian carbonate deposits are overlain by the Hangenberg shales. Depositional environments ranged from mid to outer ramp. The BU section is ca. 35 m thick and consists of lime mudstones and fine-grained turbiditic wackestones from the *Pa. rhenana* to the *Scaphignathus velifer velifer* Zone, followed by nodular limestones of the *Pa. rugosa trachytera* to the middle of the *Bispathodus ultimus* Zone and the Hangenberg shales. Depositional environments ranged from distal slope to outer ramp (Girard et al., 2017).

3. Materials

Sixty-four and forty samples were collected from the CT and BU sections, respectively (Supplementary Table). Thin sections were used for microfacies analysis. Conodonts were extracted by dissolving a fraction of the samples using 10% formic acid. All conodonts were manually picked from the insoluble residues and determined at the generic and species level. The taxonomic identification allowed establishing a detailed biostratigraphic scheme. The abundance of conodonts is high to exceptionally high, with about 600 platform elements per kg at CT and about 7000 platform elements per kg at BU. Entire and broken platform elements representing at least half of an element were counted per genus to characterize conodont biofacies in each sample (Sandberg, 1976). A fraction of these conodonts was thereafter used for oxygen isotope analyses. All approaches (microfacies, conodont biofacies, and oxygen isotope geochemistry) were performed on the same rock sample.

4. Methods

4.1. Age model

The stratigraphy of Late Devonian deposits is mostly based on conodont biostratigraphy. A revised global standard of the Famennian (Late Devonian) conodont zonation has been recently published (Spalletta et al., 2017). Zonal boundaries and duration are essentially identical to those of Ziegler and Sandberg (1990), which was used in the Global Time Scale 2012 (Becker et al., 2012) to date in absolute ages some zonal boundaries. In this study, the zonal boundaries dated in the Global Time Scale 2012 were used as anchor points to establish local linear regressions between absolute age and depth along the sections, thus providing age estimates for each sampled level. Anchor points are the basis of the following zones: *Palmatolepis triangularis, Pa. crepida*, *Pa. rhomboidea*, *Pa. marginifera marginifera*, *Pa. rugosa trachytera*, *Polygnathus styriacus*, *Palmatolepis gracilis expansa* (adapted to the zonation of Spalletta et al. 2017), and the base of the Early *praesulcata* sensu Ziegler and Sandberg (1990).

4.2. Sedimentary facies description

The description of the sedimentary facies in the Col des Tribes and Buschteich sections has been published by Girard et al. (2014) and Girard et al. (2017), respectively.

The different facies were characterized by the sedimentological and biological features from outcrops as well as thin sections, allowing an interpretation of the different depositional settings. For each section, this led to an ordering ('score') of the different samples along a theoretical proximal-distal gradient. In order to compare BU and CT, the scoring of the sedimentary facies (later on in the text: 'facies') in the two outcrops have been compiled into a single scheme.

4.3. Oxygen isotope analyses

Oxygen isotope ratios of conodont apatite can be used as a paleotemperature proxy (Joachimski and Buggisch, 2002; Joachimski et al., 2009; Luz et al., 1984). Twenty-seven conodont samples from the Buschteich section and 26 conodont samples from the Col des Tribes section have been studied for oxygen isotopes. Chemical conversion of apatite bound phosphate into trisilverphosphate (Ag_3PO_4) was performed according the method described in Joachimski et al. (2009). Oxygen isotope analyses were performed using a TC-EA (high-temperature conversion-elemental analyzer) coupled online to a ThermoFinnigan Delta V Plus mass spectrometer. 0.2 to 0.3 mg Ag_3PO_4 was weighed into silver foil and transferred to the sample carousel of the TC-EA. At 1450 °C, the silver phosphate is reduced and CO forms as the analyte gas (Vennemann et al., 2002). CO was transferred in a helium stream through a gas chromatograph via a Conflo III interface to the mass spectrometer. All values are reported in ‰ relative to V-SMOW. Samples as well as standards were generally measured in triplicate. The measurements were calibrated by performing a two-point calibration (Paul et al., 2007) using NBS 120c ($\delta^{18}O$ = 21.7‰) and a commercial Ag3PO4 (9.9‰). A laboratory standard was used as a control standard and processed together with the samples. All standards were calibrated to TU1 ($\delta^{18}O$ = +21.11‰) and TU2 (+5.45‰; Vennemann et al., 2002). The average oxygen isotope composition of the internationally distributed standard NBS 120c was measured as +21.67 ± 0.09 (1 σ; n= 5).

4.4. Conodont biofacies

Late Devonian conodont taxa were supposed to have different water depth preferences (Klapper and Barrick, 1978; Seddon and Sweet, 1971). Hence, the proportion of the different genera within a given assemblage was interpreted as a proxy of water depth (Sandberg, 1976; Seddon and Sweet, 1971). Refined biofacies

interpretations based on conodont subgenera or even species have been proposed (e.g. Lüddecke et al., 2017) but due to species evolution and replacement through time, this approach appeared difficult to apply to the relatively long record considered in the present study. During the late Frasnian to late Famennian, at least seven genera are present and can provide information about depositional environments (e.g. Corradini, 2003; Morrow, 2000; Sandberg, 1976; Seddon and Sweet, 1971). The genera that have been most clearly associated to water depth preferences are the following. (1) For deep waters, *Palmatolepis* and *Bispathodus/Branmehla/Mehlina*. It should be noted that whereas *Palmatolepis* is considered to be a specialist of offshore environments, *Bispathodus* presents wider tolerance to water depth and/or proximity to the shore (Ziegler and Sandberg 1984). (2) *Polygnathus* for intermediate water depth. (3) *Icriodus, Scaphignathus,* and *Alternognathus* for shallow waters. Due to their low abundance and similar environmental preferences, the two latter genera have been grouped for biofacies representation. Hence, in this study, the following biofacies were recognized: the palmatolepid biofacies, the palmatolepid-polygnathid biofacies, and the bispathodid-polygnathid biofacies.

4.5. Data analysis and statistics

The proportion of each genus was estimated in each sampled level based on counting (Girard et al., 2014, 2017). The description of these proportions corresponds to the conodont biofacies analysis itself. A principal component analysis (PCA on the variance-covariance matrix) was performed on these percentages to summarize the variation of all genera on few main axes. This analysis also provided a representation of the records of CT and BU on the same synthetic axes, allowing a direct comparison of the biofacies variations in the two outcrops. The contribution of each genus percentage to the axes allowed their interpretation in relation to the biofacies. The PCA was performed using the R package ade4 (Dray and Dufour, 2007). The different proxies (microfacies, oxygen isotope ratios and the first axis of the PCA on the conodont percentages) were compared using linear regression analysis in CT and BU separately, and in the combined dataset (CT+BU). To test for a secular climate evolution, the relationship between oxygen isotope values and time was tested using linear regressions in CT, BU and CT+BU. In addition, this relationship was also investigated using a linear model including as terms the age of the levels, the section and the interaction between the two

former terms. If the interaction between two terms, here age and section, is significant, this means that the relationship of the dependent variable (here, $\delta^{18}O$ values) to age have a different slope in the two sections. To test if $\delta^{18}O$ values were different in two phases of the record, t-tests were also used. All these tests were performed under R (R Core Team, 2017). An analysis of variance (ANOVA) on a linear model combining microfacies and oxygen isotopes as explanatory variables was used to assess their relative influence on conodont assemblages, estimated by the scores along the first axis of the PCA on conodont percentages. A type II ANOVA was used, because this method is invariant to ordering of the model terms and is powerful even with unbalanced datasets. This test was done using the R package ffmanova (Langsrud and Mevik, 2012).

5. Results

5.1. Age model

The absolute ages estimated in Becker et al. (2012) for some zonal boundaries served us as anchor points. A correlation with sediment thickness allowed establishing an age model for each section (Fig. 2). The observed sediment thickness includes post-depositional processes such as compaction, erosion, and diagenesis, that may affect the estimates of accumulation rates through time and between sections. With this limitation, Famennian mean accumulation rates were low in CT (5 to 7 mm/kyr^{-1}) and extremely low in BU (1 to 3 mm/kyr^{-1}). Two periods of more or less constant accumulation rates can be identified in BU: one from the *Pa. crepida* Zone to the *Sc. velifer velifer* Zone, and a second, with even lower rates, from the *Palmatolepis rugosa trachytera* Zone to the end of the Famennian. In CT, these two intervals can also be recognized, with possibly a temporary acceleration of deposition during the *Pa. marginifera marginifera* and *marginifera utahensis* Zones. The ages estimated for each sample were thereafter used to plot the variations of the conodont assemblages and of the environmental proxies. This allowed a comparison of the timing of changes in both sections.

5.2. Sedimentary facies

The sedimentary facies of BU and CT have been compiled into a single scheme. Five facies types have been distinguished based on microfacies and faunal content (Fig. 3). The interpolated scheme is summarized below and compared to the published facies at CT (Girard et al., 2014) and BU (Girard et al., 2017). Details are provided in the Supp.

Table 1. Based on these facies characteristics, the temporal variation in the depositional setting can be reconstructed. Note that all depositional environments are relatively deep, and correspond to the deepest environments found on the shelf, and that the terms 'shallow' and 'deep' are used in the context of relative shallowing or deepening. At BU only minor variations can be observed (Fig. 4A). The depositional environment, mostly corresponding to Facies 2, remained relatively deep throughout the record. Intervals with the even deeper Facies 1 can be identified during the Late Frasnian, the *Pa. crepida and termini* Zones, the *Pa. marginifera marginifera* Zone, the *Sc. velifer velifer* Zone, and the top of *Bispathodus ultimus* Zone. The CT section shows evidence for more important changes in water depth. A first shallowing episode occurred during the latest Frasnian and earliest Famennian, followed by a second, shallower episode during the *Pa. gracilis gracilis* and the *Pa. marginifera marginifera* Zones. From the top of the *Pseudopolygnathus granulosus* Zone to the end of the Famennian, conditions were constantly shallower than during the two former episodes. These shallowing trends are separated by two deepening episodes, from the *Pa. minuta minuta* to the *Pa. rhomboidea* Zone and from the *Pa. marginifera marginifera* to the *Pseudopolygnathus granulosus* Zone.

5.3. Oxygen isotopes

Oxygen isotope ratios measured on conodont apatite from CT are between +17.1 and +17.7‰ from the end Frasnian to the *Pa. crepida* zone (Fig. 4B). Values thereafter more or less gradually increase to values around 18‰ in the *Pa. marginifera utahensis* Zone. From the *Sc. velifer velifer* to the *Pa. gracilis expansa*, $\delta^{18}O$ increases to values above +19‰. A slight decrease is observed to the end of the Famennian. Oxygen isotope values of conodont apatite from BU are generally higher than values observed at CT. $\delta^{18}O$ values range from +16.4 to +16.9 ‰ from the end Frasnian to the *Pa. crepida* zone. From a minimum of +16.4 ‰ at the base of the *Pa. crepida* Zone, a trend to higher values occurs up to the *Pa. marginifera marginifera* Zone, reaching $\delta^{18}O$ values of +17.8 ‰. A brief decrease marks the first part of the *Pa. marginifera utahensis* Zone, with $\delta^{18}O$ values of around +16.7 ‰. Thereafter, up to the end of the Famennian, $\delta^{18}O$ values remain close to +17.5 ‰.

The offset in $\delta^{18}O$ between the two sections is relatively small (+0.5 to +1‰) from the *Pa. crepida* Zone to *Pa. marginifera utahensis* Zone, but increases after the *Sc. velifer velifer* Zone (+1 to +1.5 ‰). This difference in $\delta^{18}O$ translates into +6 to +6.5°C cooler temperatures in CT in case the offset is solely explained by temperature.

5.4. Conodont biofacies

The conodont biofacies follow overall comparable trends in both sections (Fig. 5; Supp. Table 1), sharing a dominance of *Palmatolepis* for most of the time up to a maximum at the base of the *Pa. marginifera marginifera* Zone (up to more than 95% of the assemblage), followed by a progressive decrease towards the end Famennian. This decrease of *Palmatolepis* was compensated almost exclusively by a rise of *Bispathodus* in CT and by a rise of both *Polygnathus* and *Bispathodus* in BU. The Frasnian assemblages were complemented by the occurrence of other genera such as *Polygnathus* and *Ancyrodella*. The *Pa. triangularis* to *Pa. minuta minuta* Zones, which are missing in BU, were marked by an increase in the abundance of *Icriodus* in CT. Another maximum in the abundance of *Icriodus* in CT is recognized in the *Pa. glabra prima* Zone. Except for the *Pa. crepida* Zone, *Icriodus* was rare in BU. In CT, a short-term rise of *Scaphignathus/Alternognathus* occurred around the *Ps. granulosus* Zone. A similar but more discrete rise is present at the base of the *Pa. rugosa trachytera* Zone in BU.

5.5. Multivariate analysis of the conodont taxa abundances

The principal component analysis performed on the proportions of the different genera allowed summarizing the biofacies variations on one main axis (PC1) expressing more than 75% of the total variance. The record of the two sections CT and BU can be directly compared on these axes. The contribution of the variables (here, the percentages of the different genera) to the axes (Fig. 6A) shows that positive values along the first axis correspond to a high proportion of *Palmatolepis* whereas negative values correspond to a high proportion of *Bispathodus.* Variations along the PC1 axis thus correspond to the replacement of *Palmatolepis* by *Bispathodus*. The second axis represents only less than 20% of variance, and mostly corresponds to variations in the proportion of *Polygnathus*. Other genera contribute very little to the two main axes, due to their rare occurrence in the records.

Representing the different levels in the first principal plane of this PCA allows for a comparison of BU and CT conodont biofacies variations (Fig. 6B-I). Most of the time, the range of values covered by samples from the two sections largely overlaps. The oldest samples (mostly Frasnian) are characterized by a peculiar diagonal distribution (Fig. 6B). Their shift in the PCA space compared to Famennian samples is due to the occurrence of genera such as *Ancyrodella* that went extinct during the Frasnian - Famennian crisis. Early Famennian levels of both sections are tightly clustered, sharing extreme positive values along the first axis, due to the overwhelming dominance of *Palmatolepis*.

In CT, a shift towards negative PC1 values is launched between the *Pa. marginifera marginifera* and *Pa. marginifera utahensis* Zones (Fig. 4C, 6E), corresponding to the onset of the decrease in the abundance of *Palmatolepis* (Fig. 5). This shift went on to reach extreme negative PC1 values as early as the *Po. styriacus* Zone (Fig. 6G, H). This change started more or less at the same time at BU, but it did not occur in a consistent manner for a while. Only towards the end of the studied interval, during the *Bispathodus ultimus* Zone, PC1 values in BU reach a range similar to the one observed in CT (Fig. 6I). This corresponded to the final decrease of *Palmatolepis* at BU, close before its extinction near the Devonian-Carboniferous boundary (Fig. 5). The consequence of this delay in the decrease of *Palmatolepis* at BU was a temporary offset between the two records of conodont genera proportions, starting during the *Ps. granulosus* Zone and persisting until the base of the *Bi. ultimus* Zone (Fig. 4C).

5.6. Comparison of paleoenvironmental proxies and conodont biofacies

As a first step, we compared the different proxies (Table 2). Facies, oxygen isotope ratios, and the first axis of the principal component analysis on the conodont percentages (later on mentioned as conodont PC1) are all significantly correlated when considering the total dataset (CT+BU). In contrast, none of the correlations is significant when considering BU. At CT, conodont PC1 is significantly correlated to facies and $\delta^{18}O$, but the two latter variables are not correlated.

The variation in the oxygen isotope ratios shows a significant secular trend, the relationship of $\delta^{18}O$ and age being significant in the CT, BU and CT+BU datasets. In the linear model investigating the variation of $\delta^{18}O$ depending on age in the two sections, the interaction term between $\delta^{18}O$ and age is not significant. This means that

the slope of the regression is the same in the two sections. While the two sections display a similar increase in $\delta^{18}O$ when considering the whole record, from the end Frasnian to the Late Famennian, the records of CT and BU do not follow a similar pattern after the *Pa. marginifera utahensis* Zone (Fig. 4B). The oxygen isotope ratios increase in CT but remain stable in BU. To test for such a discrepancy between the records of the two sections, we performed t-tests between oxygen isotope values of the period preceding and following the apparent shift in CT. The difference in $\delta^{18}O$ is indeed statistically significant in CT (t-test [from *Pa. rhomboidea to Sc. velifer velifer*, n =8] vs. [from *Pa. rugosa trachytera* to *Bi. ultimus*, n = 7], P = 0.0026). In contrast, the $\delta^{18}O$ values of the same periods do not differ in BU (t-test [n = 6 and 11], P = 0.3443).

Finally, to investigate whether $\delta^{18}O$ or facies better explains the variation of the conodont genera, linear models with conodont PC1 as dependent variable, and $\delta^{18}O$ and facies as independent factors were considered (Table 3). The interaction term between both factors ($\delta^{18}O$ and facies) is weak (p = 0.0311 for CT+BU) or not significant (for CT and BU separately). This term was therefore discarded from the models. Facies and $\delta^{18}O$ are significant explanatory variables of conodont biofacies when considering CT and BU together, and CT alone. Facies explains more than three times more variance than $\delta^{18}O$ in both cases. None has significant effect in BU.

6. Discussion

Our detailed oxygen isotope records generally show an increase in $\delta^{18}O$ in both sections from the end Frasnian to end Famennian, coherent with described global cooling during this time interval (Joachimski et al., 2009). However, in details, the two records show different temperature variations from the *Pa. rugosa trachytera* Zone to end Famennian. While temperature remained more or less stable throughout the Famennian in the BU section (Saxo-Thuringia), it decreased in the CT section (Montagne Noire) towards *Sc. velifer velifer* Zone. This difference in $\delta^{18}O$ between CT and BU is mirrored by different sea-level variations in CT and BU, as pointed out by facies description. Given these differences between the paleoenvironmental settings of the two areas, conodont biofacies delivered remarkably similar records, questioning the role of the paleoenvironmental forcing on conodont assemblages.

6.1. Paleotemperature variations: a global trend mitigated by paleogeography?

A global temperature trend has been sketched for the Late Devonian (McGhee, 2013), based on variations in $\delta^{18}O$ of conodont apatite (Joachimski et al., 2009). This composite record showed a rapid succession of cooling and warming pulses around the Frasnian-Famennian boundary (Balter et al., 2008; Joachimski and Buggisch, 2002; Huang et al. 2018). After a warm period during the *triangularis* Zone, a progressive long-term cooling was proposed for the rest of the Famennian (Joachimski et al., 2009), culminating into a period with stable ice caps during the early Carboniferous (Buggisch et al. 2008). As for some other oxygen isotope studies in the Paleozoic, our isotope records are based on conodont apatite, thus tracing the environment where the conodont lived. Furthermore, all analyses were performed on the same genus, *Palmatolepis*, avoiding the problem that different oxygen isotope values in the two sections may be due to analyses on genera with different habitat preferences. Our results support a long-term cooling, since the two sections displayed a parallel increase in the oxygen isotope ratio from the end Frasnian to end Famennian, although more pronounced in CT than in BU. An offset, however, exists between the records of the two sections, with BU constantly showing lower $\delta^{18}O$ values than CT. Based on the paleogeographic reconstruction (Fig. 1), BU and CT were both in the subtropical zone. The constant offset between the two records can thus hardly be explained by a latitudinal difference. Possibly, CT being positioned further towards the Paleotethys (Franke et al., 2017), it might have been more exposed to the colder water masses of the open Paleotethys Ocean and Paleo-Adria epicontinental sea.

Beyond the cooling trend registered in both sections from the *Pa. crepida* to *Pa. marg. marginifera* Zone, the oxygen isotope records from BU and CT show differing trends after the *Pa*. *marginifera utahensis* Zone. This pattern is also seen in other sections studied by Joachimski et al. (2009). For example, in the La Serre section (Montagne Noire) an increase in $\delta^{18}O$ is reported between the *marginifera marginifera* and *Sc. velifer velifer* Zones, similar and synchronous to the one documented in CT. In contrast in the Kahlleite section (Saxo-Thuringian area) $\delta^{18}O$ is relatively stable as in BU (Fig. 4). The difference in the $\delta^{18}O$ records of the BU and CT sections after the *Pa. marginifera utahensis* Zone is thus confirmed at the regional scale, suggesting that the paleogeographic position of the two microcontinents may have controlled the temperature changes.

462 Paleogeographic reconstructions suggest that Saxo-Thuringia was located close
463 to the first zone of closure of the Rheic Ocean (Franke et al., 2017). As the closure of the
464 Rheic Ocean progressed during the Famennian, the area might have been influenced by
465 a relative restriction of the water masses exchanges between the Rheic Ocean and the
466 Paleotethys Ocean. The upper water column temperatures might have been warmer
467 than in the open sea, as e.g. nowadays in the Caribbean Sea, the Persian Gulf, or the
468 eastern Mediterranean (see for instance Schlitzer, 2006; Schmidt et al., 2016),
469 dampening the effects of the global cooling, especially in a subtropical area. In contrast,
470 the CT section and more generally the Armorica area, being opened towards the
471 Paleotethys Ocean, would have been exposed to the Paleotethys water circulation and
472 global temperature trends, as established by Joachimski et al. (2009). This
473 interpretation is corroborated by the fact that Late Famennian $\delta^{18}O$ values recorded in
474 the Carnic Alps (Paleo-Adria, Fig. 1; *Pa. gracilis expansa* and *Bi. ultimus* Zones: ~18,3 ‰;
475 Kaiser et al., 2006, 2008), and hence also in an environment open towards the
476 Paleotethys (Paleo-Adria on Fig. 1), were closer to those recorded at CT than at BU.
477
478 *6.2. Water depth variations, combination of eustatic trends and local tectonics*
479 Sea-level variations correspond to a high-stand during the end of the Frasnian,
480 followed by a progressive sea-level fall during the Famennian (Haq and Schutter, 2008;
481 Johnson et al., 1985, 1996; Sandberg et al., 2002). These variations appear to have
482 occurred world-wide, thus pointing to eustatic trends (Johnson et al., 1985, 1996). In
483 this context, a decrease in water depth should coincide with increasing ice volume, a
484 glacio-eustatic sea-level fall and a temperature decrease. In the CT section, a regressive
485 trend and a cooling are indeed registered, but they do not occur in parallel with the
486 shallowing clearly postponing the shift towards colder temperature. Another
487 discrepancy with the expectation is that both the temperature and water depth decrease
488 do not seem to have occurred in a progressive manner, but rather abruptly. Possibly,
489 paleogeographic and/or tectonic events might have temporarily mitigated the
490 expression of the long-term trend in CT. Water depth variations in BU do not follow this
491 global trend. In BU, the depositional environment remained deep throughout the
492 Famennian, and tectonic activity has been invoked to explain this discrepancy (Girard et
493 al., 2017). The paleogeographic position of Saxo-Thuringia, close to Baltica and hence

one of the first microcontinent to collide with it, matches well with active tectonics causing a local departure from the eustatic trend.

6.3. Congruent variations of the conodont assemblages despite discrepant paleoenvironmental settings

In contrast to the different patterns of temperature variation after the *Pa. marginifera utahensis* Zone, and differences in water depth records in CT and BU, trends in conodont biofacies are quite comparable. Both sections reflect a dominance of *Palmatolepis* for most of the Famennian with a decline starting in the *Pa. marginifera marginifera* Zone. If the difference between the environments at CT and BU had any impact on the conodont assemblages, it was only minor and corresponded to a transient offset between the two conodont records. However, conodont biofacies are advocated to be mostly driven by water depth variations, due to the habitat preferences of the different conodont genera (Sandberg, 1976; Seddon and Sweet, 1971). Initially, two ecological models, i.e. depth stratification vs. lateral segregation, were proposed (Klapper and Barrick, 1978; Seddon and Sweet, 1971). The depth-stratification model implies that specific conodont taxa inhabited different depth zones within the water column, whilst the lateral segregation model proposes that bottom-dwelling taxa were dominantly controlled by habitat properties near the sediment–water interface. The abundant occurrence of conodonts during anoxic events precludes a benthic or nektobenthic lifestyle. During the Frasnian and the Famennian, genera supposed to have "shallow preferences "(e.g. *Icriodus*) and "preferences for deep environments" (e.g. *Palmatolepis*) have been shown to share similar oxygen isotope signatures, suggesting that they were living in the same water-mass (Joachimski et al., 2009). This supports the interpretation that all genera were at that time living close to the surface, but occupying proximal or distal locations. The higher proportion of the offshore surface dweller genus *Palmatolepis* in the sediments from BU than from CT is coherent with the more off-shore depositional setting in BU. The decrease of the genus *Palmatolepis* after the *Pa. marginifera marginifera* Zone is also coherent with the regressive trend characterizing the Famennian. Possibly, before the *Sc. velifer velifer* Zone, water depth was constantly deep enough to favor the dominance of this offshore surface dweller genus. However, if a direct forcing of water depth on conodont distribution is assumed, conodont biofacies at BU should have been relatively stable through time, and depart more clearly from the

trend observed at CT. This suggests that the response of conodont assemblages to water depth was mitigated by other factors. Possibly, the eustatic regressive trend was disadvantageous to the offshore surface dweller genus *Palmatolepis* at a worldwide scale, triggering its global decline. Ultimately, it would have even declined in constantly deep environments such as BU, although with a time lag suggesting that it temporarily found there a refuge of favorable environments.

6.4. Relationship between the different paleoenvironmental proxies

The three paleoenvironmental proxies considered here (sedimentary facies, oxygen isotopes, and conodont biofacies) are potentially interrelated: oxygen isotopes are temperature proxies; facies traces water depth and distance to the shore, related to temperature trends through eustatic variations; and conodont biofacies are interpreted as related to water depth due to habitat preferences of the different conodont genera along a proximal-distal gradient in the surface waters. No relationship between these proxies is evident in BU, but this absence of a significant correlation is probably due to the reduced range of variation in the oxygen isotope ratios and facies observed in this section. Oxygen isotopes and facies are correlated when considering the total data set. However, conodont PC1 displays a stronger relationship with oxygen isotopes on the one hand, and with facies on the other hand, than oxygen isotopes with facies: the percentage of variance explained is larger, leading to significant relationships in CT as well (Table 2). Considering the percentage of variance explained, facies furthermore appears as a better explanatory variable for conodont variations than $\delta^{18}O$. The sedimentary facies trace directly the depth of the depositional environment but the relevance of this approach has been discussed due to the paucity of preserved biotas in old sediments (e.g. see Flügel, 2004; Lüddecke et al., 2017). The correlation evidenced between facies and conodont biofacies is nevertheless coherent with the interpretation of conodont genera distribution being controlled by water depth, along a proximal-distal gradient (Klapper and Barrick, 1978). The fact that conodont biofacies respond earlier and more progressively to the global regressive trend may be due to the fact that CT and BU being located in outer shelf environments, the decrease in water depth should be important enough to cause a change in the facies.

6.5. Paleogeography and paleoenvironment: a complex interplay

Many studies focused on global environmental trends in the Devonian (e.g. Goddéris and Joachimski, 2004; Haq and Schutter, 2008; Miller et al., 2005; Sandberg et al., 1988; Wilson and Norris, 2001), especially during the Late Devonian for which environmental conditions have been suggested to be homogeneous within the subtropical zone, and the marine faunas to be cosmopolitan. However, our results, based on two detailed 13 My long records, indicated different paleoenvironmental changes in BU and CT. After the end of the *Pa. marginifera utahensis* Zone, the cooling and the regressive trend found little expression in BU compared to CT, but these differences are only weakly mirrored in the conodont assemblages. The differences in the temperature records of CT and BU are not only observed in the two studied sections, but registered as well in two other sections (Kahlleite and La Serre) from the Saxo-Thuringian and Montagne Noire areas (Joachimski et al., 2009), respectively. We propose that the deviation of the BU record from what we interpret as the global trend may be attributed to the paleogeography of the Saxo-Thuringian area, where a progressive restriction of water-mass exchange possibly accompanied the closing of the seaway between the remnant Rheic and Paleotethys oceans. This restricted paleogeography together with a subtropical location might have favored the persistence of warm conditions in the sea-waters where conodonts lived despite the onset of global cooling. Such setting should also have been prone to active tectonics overprinting the eustatic trend. Not mutually exclusive, the closure of the Rheic Ocean itself might have contributed to the global climate change, by interrupting the circum-equatorial circulation (see for instance for the closure of the Panama Isthmus: Bartoli et al., 2005 and Haug and Tiedemann, 1998), but this remains speculative and challenges further studies.

Increasing the geographic coverage of a multi-proxy approach, such as the one outlined here, may thus provide relevant information to better constrain paleogeographic reconstructions characterized by a complex distribution of land and water masses, as e.g. in the Late Devonian. This key step will contribute to a better understanding of the complex interplay between paleogeography, climate, and biotic response and go beyond the tempting, but misleading, view of global trends affecting the different regions in a relatively homogeneous manner.

7. Conclusions

This study presents a detailed comparison of two Famennian successions in the Montagne Noire (France) and Saxo-Thuringia (Germany). During the Famennian, both areas were located in the subtropical realm and were part of two microcontinents bracketed between the remnant Rheic Ocean and Gondwana. Based on the same rock samples, paleotemperatures were estimated using oxygen isotopes of conodont apatite, depositional environments were assessed based on sedimentary facies, and the response of conodont assemblages was evaluated using conodont biofacies. Applying a principal component analysis to biofacies data provided a synthetic axis summarizing the biofacies variations along the two sections. This allowed for a quantitative comparison of the biofacies records with paleoenvironmental proxies.

During the Famennian, both the Montagne Noire and Saxo-Thuringia display a parallel increase in the oxygen isotope ratios translating into long-term cooling. However, during the Late Famennian, temperatures remained stable in Saxo-Thuringia, leading to a temperature offset compared to the Montagne Noire record. The Late and latest Famennian are also characterized by a regressive trend which was found to be well expressed in the sedimentary facies in the Montagne Noire, but not in Saxo-Thuringia, where the depositional environment remained deep throughout. Despite these environmental differences, conodont biofacies were rather comparable in the Montagne Noire and Saxo-Thuringia. A temporary offset however suggested that *Palmatolepis*, the typical off-shore surface dwelling taxon, was abundant for a longer time period in the deep Saxo-Thuringian environment. The environmental differences between the two areas are tentatively explained by their paleogeographic location. The Saxo-Thuringian microplate is interpreted as located close to the point of first closure of the Rheic Ocean and thus might have been influenced by active tectonism and a restricted water mass exchange, blurring the impact of the long-term trends in this setting.

Acknowledgments

We thank D. Delmas and C. Nevado (Lyon, France) who produced the thin-sections and Raimund Feist (Montpellier, France), Dieter Weyer (Berlin, Germany) and Konrad Bartzsch (Saafeld, Germany) for their contribution during field trips. The research was supported by the ANR Project ECODEV (ANR-13-BSV7-005). This is publication ISEM 2018-XXX.

625
626 **References**
627

628 Balter, V., Renaud, S., Girard, C., Joachimski, M.M., 2008. Record of climate-driven
629 morphological changes in 376 Ma Devonian fossils. Geology 36, 907-910.
630 Bartoli, G., Sarnthein, M., Weinelt, M., Erlenkeuser, H., Garbe-Schônberg, C.-D., Lea, D.W.,
631 2005. Stable isotope analysis and temperature reconstruction data from DSDP Hole 94-
632 609B and ODP Hole 162-984B, Supplement to: Bartoli, G. et al. (2005): Final closure of
633 Panama and the onset of northern hemisphere glaciation. Earth Planet. Sci. Lett., 237,
634 33-44, https://doi.org/10.1016/j.epsl.2005.06.020. PANGAEA.
635 Becker, R.T., 1993. Anoxia, eustatic changes, and upper Devonian to lowermost
636 Carboniferous global ammonoid diversity, in: House, M.R. (Ed.), The Ammonoidea:
637 Environment, Ecology, and Evolutionary Change. Systematics Association Special
638 Volume, Oxford, pp. 115-163.
639 Becker, R.T., Gradstein, F.M., Hammer, O., 2012. The Devonian Period, in: Gradstein, F.M.,
640 Ogg, J.G., Schmitz, M.D., Ogg, G.M. (Eds.), The Geologic Time Scale 2012. Elsevier,
641 Oxford, pp. 559-602.
642 Becker, R.T., House, M.R., 1997. Sea-level changes in the Upper Devonian of the Canning
643 Basin, Western Australia. Cour. Forsch.-Inst. Senckenberg 199, 126-146.
644 Becker, R.T., Kaiser, S.I., Aretz, M., 2016. Review of chrono-, litho- and biostratigraphy
645 across the global Hangenberg Crisis and Devonian–Carboniferous Boundary, in:
646 Becker, R.T., Koenigshof, P., Brett, C.E. (Eds.), Devonian Climate, Sea Level and
647 Evolutionary Events. The Geological Society of London, London, 423, 355-386.
648 Belka, Z., Wendt, J., 1992. Conodont biofacies patterns in the Kellwasser Facies (upper
649 Frasnian/lower Famennian) of the eastern Anti-Atlas, Morocco. Palaeogeogr.
650 Palaeoclimatol. Palaeoecol. 91, 143-173.
651 Brett, C., Allison, P.A., 1998. Paleontological Approaches to the Environmental
652 Interpretation of Marine Mudrocks, in: Schieber, Zimmerle, Sethi (Eds.), Shales and
653 Mudstones. E Schweizerbartsche Verlagsbuchandlung (Nagel u. Obermiller), Stuttgart,
654 pp. 301-349.
655 Buggisch, W., Joachimski, M. M., Sevastopulo, G., Morrow, J.R. 2008. Mississippian $\delta^{13}C_{carb}$
656 and conodont apatite $\delta^{18}O$ records — Their relation to the Late Palaeozoic Glaciation,
657 Palaeogeogr. Palaeoclimatol. Palaeoecol. 268(3-4), 273-292, doi:
658 doi:10.1016/j.palaeo.2008.03.043.

659 Caputo, M.V., Melo, J.H.G., Streel, M., Isbell, J.L., 2008. Late Devonian and Early
660 Carboniferous glacial records of South America, in: Fielding, C.R., Frank, T.D., Isbell, J.L.
661 (Eds.), The Geological Society of America, Special Paper. Geol. Soc. America, pp. 161-
662 173.
663 Corradini, C., 2003. Late Devonian (Famennian) conodonts from the Corona Mizziu
664 Sections near Villasalto (Sardinia, Italy). Palaeontographia Italica 89, 65-116.
665 Dray, S., Dufour, A.-B., 2007. The ade4 package: implementing the duality diagram for
666 ecologists. J. Stat. Softw 22, 1-20.
667 Eckelmann, K., Nesbor, H.-D., Königshof, P., Linnemann, U., Hofmann, M., Lange, J.-M.,
668 Sagawe, A., 2014. Plate interactions of Laurussia and Gondwana during the formation
669 of Pangaea — Constraints from U–Pb LA–SF–ICP–MS detrital zircon ages of Devonian
670 and Early Carboniferous siliciclastics of the Rhenohercynian zone, Central European
671 Variscides. Gondwana Research 25, 1484-1500.
672 Feist, R., Becker, R.T., 1997. Discovery of Famennian trilobites in Australia (Late
673 Devonian, Canning Basin, NW Australia). Geobios M.S. 20, 231-242.
674 Flügel, E., 2004. Microfacies of carbonate rocks. Analysis, Interpretation and Application.
675 Springer Verlag, Berlin, Heildelberg, NewYork.
676 Franke, W., Cocks, L.R.M., Torsvik, T.H., 2017. The Palaeozoic Variscan oceans revisited.
677 Gondwana Res. 48, 257-284.
678 Girard, C., Feist, R., 1997. Eustatic trends in conodont diversity across the
679 Frasnian/Famennian boundary in the stratotype area, Montagne Noire, France. Lethaia
680 29, 329-337.
681 Girard, C., Cornée, J.-J., Corradini, C., Fravalo, A., Feist, R., 2014. Palaeoenvironmental
682 changes at Col des Tribes (Montagne Noire, France), a reference section for the
683 Famennian of north Gondwana-related areas. Geol. Mag. 151, 864-884.
684 Girard, C., Cornée, J.-J., Charruault, A.-L., Corradini, C., Weyer, D., Bartzsch, K., Joachimski,
685 M.M., Feist, R., 2017. Conodont biostratigraphy and palaeoenvironmental trends during
686 the Famennian (Late Devonian) in the Thuringian Buschteich section (Germany).
687 Newsl. Stratigr. 50, 71-89.
688 Goddéris, Y., Joachimski, M.M., 2004. Global change in the Late Devonian: modelling the
689 Frasnian-Famennian short-term carbon isotope excursions. Palaeogeogr.
690 Palaeoclimatol. Palaeoecol. 202, 309-329.

691 Haq, B.U., Schutter, S.R., 2008. A chronology of Paleozoic sea-level changes. Science 322,
692 64-68.
693 Hartenfels, S., 2011. Die globalen Annulata-Events und die Dasberg-Krise (Famennium,
694 Oberdevon) in Europa und Nord-Afrika – hochauflösende Conodonten-Stratigraphie,
695 Karbonat-Mikrofazies, Paläoökologie und Paläodiversität. Münstersche Forschungen
696 zur Geologie und Paläontologie, Paleontologia e Stratigrafia 115, 141-158.
697 Hartenfels, S., Becker, R.T., 2009. Timing of the global Dasberg Crisis – implications for
698 Famennian eustasy and chronostratigraphy. Palaeontographica Americana 63, 71-97.
699 Hartenfels, S., Becker, R.T. 2017. The global Annulata Events: review and new data from
700 the Rheris Basin (northern Tafilalt) of SE Morocco, in: Becker, R.T., Koenigshof, P.,
701 Brett, C. (Eds.), Devonian Climate, Sea Level and Evolutionary Events. Geological
702 Society, London, Special Publications 423, http://doi.org/10.1144/SP423.1.
703 Haug, G.H., Tiedemann, R., 1998. Stable carbon and oxygen isotope ratios of Cibicidoides
704 wuellerstorfi, and CaCO3 and sand content of ODP Hole 165-999A, Supplement to:
705 Haug, GH; Tiedemann, R (1998): Effect of the formation of the Isthmus of Panama on
706 Atlantic Ocean thermohaline circulation. Nature, 393, 673-676,
707 https://doi.org/10.1038/31447. PANGAEA.
708 House, M.R., 1985. Correlation of mid-Palaeozoic ammonoid evolutionary events with
709 global sedimentary perturbations. Nature 313, 17-22.
710 Huang, C., Joachimski, M.M., Gong, Y., 2018. Did climate changes trigger the Late
711 Devonian Kellwasser crisis? Evidence from a high-resolution $\delta^{18}O_{PO4}$ record from South
712 China. Earth Planet. Sci. Letters 495, 174-184.
713 Isaacson, P.E., DÌaz-Martinez, E., Grader, G.W., Kalvoda, J., Babek, O., Devuyst, F.X., 2008.
714 Late Devonian-earliest Mississippian glaciation in Gondwanaland and its
715 biogeographic consequences. Palaeogeogr. Palaeoclimatol. Palaeoecol. 268, 126-142.
716 Joachimski, M., Buggisch, W., 2002. Conodont apatite $\delta^{18}O$ signatures indicate climatic
717 cooling as a trigger of the Late Devonian mass extinction. Geology 30, 711-714.
718 Joachimski, M.M., van Geldern, R., Breisig, S., Buggisch, W., Day, J., 2004. Oxygen isotope
719 evolution of biogenic calcite and apatite during the Middle and Late Devonian. Int. J.
720 Earth Sci 93, 542-553.
721 Joachimski, M.M., Breisig, S., Buggisch, W., Talent, J.A., Mawson, R., Gereke, M., Morrow,
722 J.R., Day, J., Weddige, K., 2009. Devonian climate and reef evolution: Insights from
723 oxygen isotopes in apatite. Earth Planet. Sci. Lett. 284, 599-609.

724 Johnson, J.G., Klapper, G., Sandberg, C.A., 1985. Devonian eustatic fluctuations in
725 Euramerica. Geol. Soc. Am. Bull. 96, 567-587.
726 Johnson, J.G., Klapper, G., Elrick, M., 1996. Devonian transgressive-regressive cycles and
727 biostratigraphy, Northern Antelope Range, Nevada: establishment of reference
728 horizons for global cycles. Palaios 11, 3-14.
729 Kaiser, S.I., Steuber, T., Becker, R.T., Joachimski, M.M., 2006. Geochemical evidence for
730 major environmental change at the Devonian-Carboniferous boundary in the Carnic
731 Alps and the Rhenish Massif. Palaeogeogr. Palaeoclimatol. Palaeoecol. 240, 146-160.
732 Kaiser, S.I., Steuber, T., Becker, R.T., 2008. Environmental change during the Late
733 Famennian and Early Tournaisian (Late Devonian–Early Carboniferous): implications
734 from stable isotopes and conodont biofacies in southern Europe. Geol. J. 43, 241-260.
735 Kaiser, S.I., Aretz, M., Becker, R.T., 2015. The global Hangenberg Crisis (Devonian-
736 Carboniferous transition): a review of a first order mass extinction, in: Becker, R.T.,
737 Königshof, P., Brett, C.E. (Eds.), Devonian climate, sea level and evolutionay events.
738 Geol. Soc. Spec. Publ., London 423, 387-437.
739 Klapper, G., Barrick, J.E., 1978. Conodont ecology: pelagic versus benthic. Lethaia 11, 15-
740 23.
741 Korn, D., 2004. The mid-Famennian ammonoid succession in the Rhenish Mountains: the
742 "*annulata* Event" reconsidered. Geological Quarterly 48, 245-252.
743 Korn, D., De Baets, K., 2015. Biogeography of Paleozoic ammonoids, in: Klug, C., Korn, D.,
744 De Baets, K., Kruta, I., Mapes, R.H. (Eds.), Ammonoid Paleobiology: From
745 macroevolution to paleogeography. Springer, New York, pp. 299-328.
746 Langsrud, Ø., Mevik, B.-H., 2012. ffmanova: Fifty-fifty MANOVA, https://CRAN.R-
747 project.org/package=ffmanova.
748 Lüddecke, F., Hartenfels, S., Becker, R.T., 2017. Conodont biofacies of a monotonous
749 middle Famennian pelagic carbonate succession (Upper Ballberg Quarry, northern
750 Rhenish Massif). Palaeobio. Palaeoenv. 97, 591–613.
751 Luz, B., Kolodny, Y., Kovak, J., 1984. Oxygen isotope variations in phosphate of biogenic
752 apatites, III. Conodonts. Earth Planet. Sci. Lett. 69, 255-262.
753 McGhee, G.R.J., 1996. The Late Devonian Mass Extinction - The Frasnian/Famennian
754 crisis. Columbia University Press, New York.
755 McGhee, G.R., Jr., 2013. When the invasion on land failed: the legacy of the Devonian
756 extinctions. Columbia University Press, New-York.

757 Miller, K.G., Kominz, M.A., Browning, J.V., Wright, J.D., Mountain, G.S., Katz, M.E.,
758 Sugarman, P.J., Cramer, B.S., Christie-Blick, N., Pekar, S.F., 2005. The Phanerozoic
759 Record of Global Sea-Level Change. Science 310, 1293–1298.
760 Morrow, J., 2000. Shelf-to-basin lithofacies and conodont paleoecology across Frasnian-
761 Famennian (F-F, mid-Late Devonian) boundary, Central Great Basin (Western U.S.A.).
762 Cou. Forsch.-Inst. Senckenberg 219, 1-57.
763 Mottequin, B., Brice, D., Legrand-Blain, M., 2013. Biostratigraphic significance of
764 brachiopods near the Devonian–Carboniferous boundary. Geol. Mag. 151, 216-228.
765 Paul, D., Skrzypek, G., Forizs, I., 2007. Normalization of measured stable isotope
766 composition to isotope reference scale – a review. Rapid Comm. Mass Spectr. 21, 3006-
767 3014.
768 R Core Team, 2017. R: A language and environment for statistical computing. R
769 Foundation for Statistical Computing, Vienna, Austria. URL https://www.R-
770 project.org/.
771 Sandberg, C.A., 1976. Conodont biofacies of late Devonian *Polygnathus styriacus* Zone in
772 western United States, in: Barnes, C.R. (Ed.), Conodont Paleoecology. Geol. Assoc.
773 Canada spec. Pap., Montreal, pp. 171-186.
774 Sandberg, C.A., Ziegler, W., Dreesen, R., Butler, J.L., 1988. Late Frasnian mass extinction:
775 conodont event stratigraphy, global changes, and possible causes. Cour. Forsch.-Inst.
776 Senckenberg 102, 263-307.
777 Sandberg, C.A., Morrow, J.R., Ziegler, W., 2002. Late Devonian sea-level changes,
778 catastrophic events, and mass extinctions. Geol. Soc. America Spec. Pap. 356, 473-487.
779 Schindler, E. 1993. Event-stratigraphic markers within the Kellwasser Crisis near the
780 Frasnian/Famennian boundary (Upper Devonian) in Germany. Palaeogeogr.
781 Palaeoclimatol. Palaeoecol. 104, 115-125.
782 Schlitzer, R., 2006. Ocean data view - 3.1.0. http://odv.awi.de
783 Schmidt, D., Caromel, A., Seki, O., Rae, J.W.B., Renaud, S., 2016. Morphological response of
784 planktic foraminifers to habitat modifications associated with the emergence of the
785 Isthmus of Panama. Mar. Micropaleontol. 128, 28-38.
786 Seddon, G., Sweet, W.C., 1971. An ecologic model for conodonts. J. Paleont. 45, 869-880.
787 Spalletta, C., Perri, M.C., Over, D.J., Corradini, C., 2017. Famennian (Upper Devonian)
788 conodont zonation: revised global standard. Bull. Geosci. 92, 1-27.

789 Stampfli, G.M., Hochard, C., Vérard, C., Wilhem, C., vonRaumer, J., 2013. The formation of
790 Pangea. Tectonophysics 593, 1-19.
791 Vennemann, T.W., Fricke, H.C., Blake, R.E., O'Neil, J.R., Colman, A., 2002. Oxygen isotope
792 analysis of phosphates: a comparison of techniques from analysis for Ag3PO4. Chem.
793 Geol. 185, 321-336.
794 Walliser, O.H., 1996. Global events and event stratigraphy. Springer Verlag, Berlin,
795 Heidelberg, New York.
796 Wilson, P.A., Norris, R.D., 2001. Warm tropical ocean surface and global anoxia during
797 the mid-Cretaceous period. Nature 412, 425-429.
798 Ziegler, W., 1962. Taxionomy und Phylogenie oberdevonischer Conodonten und ihre
799 stratigraphische Bedeutung. Abhandlungen des hessischen Landesamtes für
800 Bodenforschung 38, Wiesbaden, 166p.
801 Ziegler, W., Sandberg, C.A., 1984. *Palmatolepis*-based revision of upper part of standard
802 Late Devonian conodont zonation, in: Clark, D.L. (Ed.), Conodont biofacies and
803 provincialism. Geological Society of American special Paper, Boulder/Colorado, pp.
804 179-194.
805 Ziegler, W., Sandberg, C.A., 1990. The late Devonian standard conodont zonation. Cour.
806 Forsch.-Inst. Senckenberg 121, 1-115.

Figure captions

Figure 1. Paleogeographic reconstruction during the latest Famennian (simplified after Franke et al. 2017). BU: Buschteich; CT: Col des Tribes. Rectangles: investigated areas.

Figure 2. Age model allowing comparison of carbonate production rates between Buschteich (BU; red circles) and Col des Tribes (CT; green diamonds). Depth is given in meters. Conodont zonations according Ziegler and Sandberg (1990) on the right and Spalletta et al. (2017) on the left, absolute ages based on Becker et al. (2012). Each symbol corresponds to a sampled level. FRS: Frasnian. *Pa.*: *Palmatolepis*; *del.*: *delicatula*; *gl.*: *glabra*; *marg.*: *marginifera*; *gr.*: *gracilis*; *Sc.*: *Scaphignathus*; *v.*: *velifer*; *r.*: *rugosa*; *Ps.*: *Pseudopolygnathus*; *Bi.*: *Bispathodus*, *ac.*: *aculeatus.* In grey, zones which were not recognized in both sections.

Figure 3. Depositional model for the Col des Tribes (CT) and Buschteich (BU) sections during the Famennian.

Figure 4. Famennian environmental changes and conodont assemblage variations in the Buschteich section (BU; Saxo-Thuringia) and Col des Tribes section (CT; Montagne Noire). A: Facies distribution for CT and BU from the deepest (1) to the shallowest (5). B: $\delta^{18}O$ in CT and BU samples, compared with data of Joachimski et al. (2009) from Thuringia (Kahlleite, blue circles) and the Montagne Noire (La Serre; grey diamonds). C. Variations of conodont assemblage through time depicted as variations along the first axis of the PCA on conodont genera percentages. Green diamonds: CT; red circles: BU. Abbreviations: see Figure 2.

Figure 5. Conodont biofacies in CT and BU (after Girard et al. 2014; 2017). The proportions have been plotted again the age model. Note the absence of data (Gap) for the *Pa. linguiformis* to *Pa. crepida* zones at BU (white rectangle). *Scaphignathus and Alternognathus*: *Sc.*, *Siphonodella*: *Si.* on the figure.

Figure 6. Principal component analysis of the variations in the percentages of the conodont genera in BU and CT. The first two axes of the PCA are represented (PC1 = 77.5%; PC2 = 18.3%). Upper left panel: contribution of the percentages of the different genera to the first two PC axes. Next panels: distribution of the different levels in the plane defined by the first two PC axes (PC1 = 77.5%; PC2 = 18.3%). The representation has been split by temporal zones (because of their limited sampling, *Pa. triangularis* to *Pa. gl. pectinata* Zones have been grouped). Each dot represents the assemblage in a level. CT: green diamonds, green diamonds with black outlines: levels from the *triangularis* and *minuta minuta* Zones; BU: red circles. *Pa.*: *Palmatolepis*; *gl.*: *glabra*; *gr.*: *gracilis*; *marg.*: *marginifera*; *Sc.*: *Scaphignathus*; *v.*: *velifer*; *r.*: *rugosa*; *Ps.*: *Pseudopolygnathus*; *Po.*: *Polygnathus; Bi.*: *Bispathodus.*

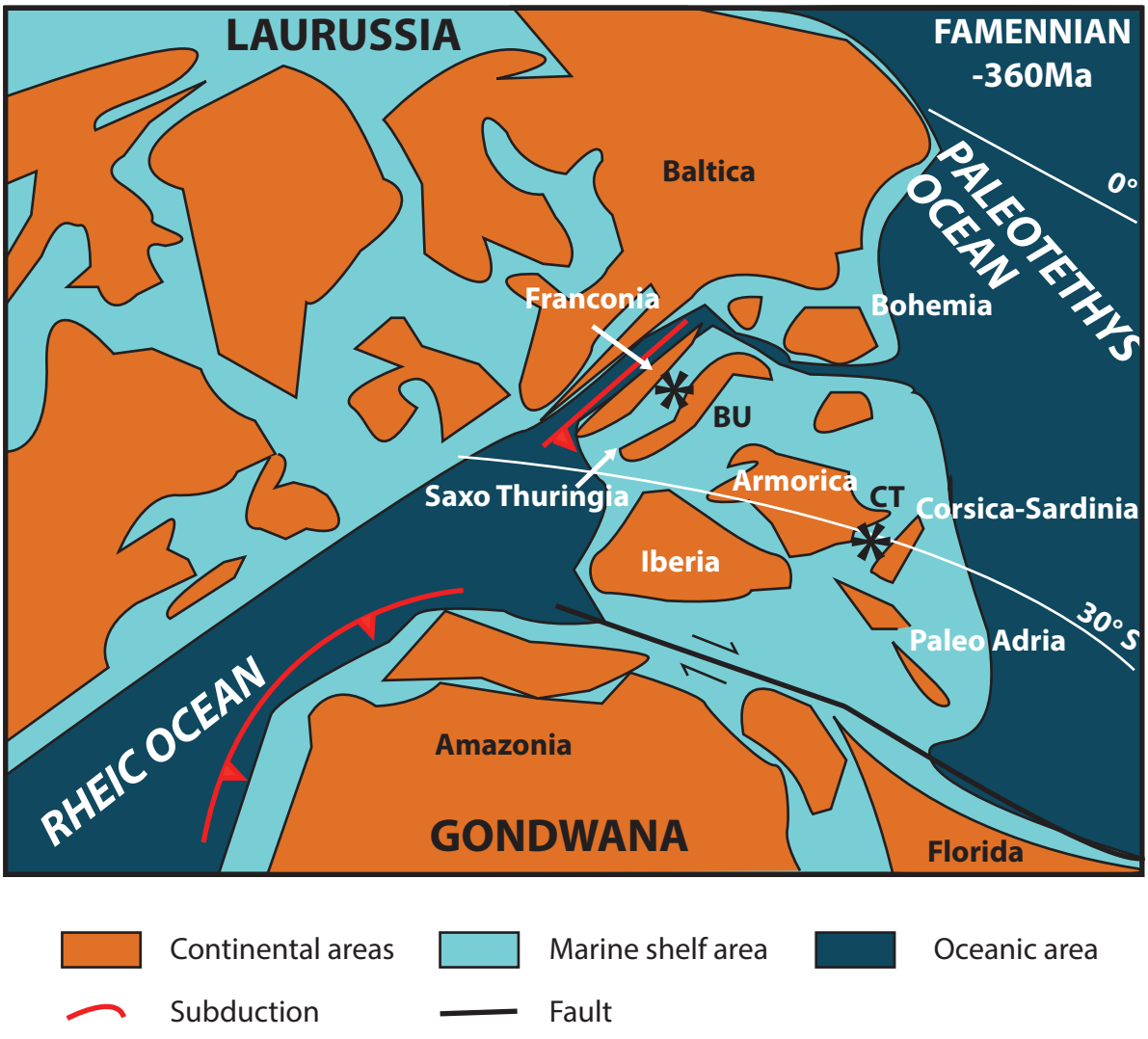
LAURUSSIA
FAMENNIAN
-360Ma
Baltica
PALEOTETHYS OCEAN
0°
Franconia
Bohemia
BU
Armorica
CT
Corsica-Sardinia
Saxo Thuringia
Iberia
30° S
Paleo Adria
RHEIC OCEAN
Amazonia
GONDWANA
Florida
Continental areas
Marine shelf area
Oceanic area
Subduction
Fault

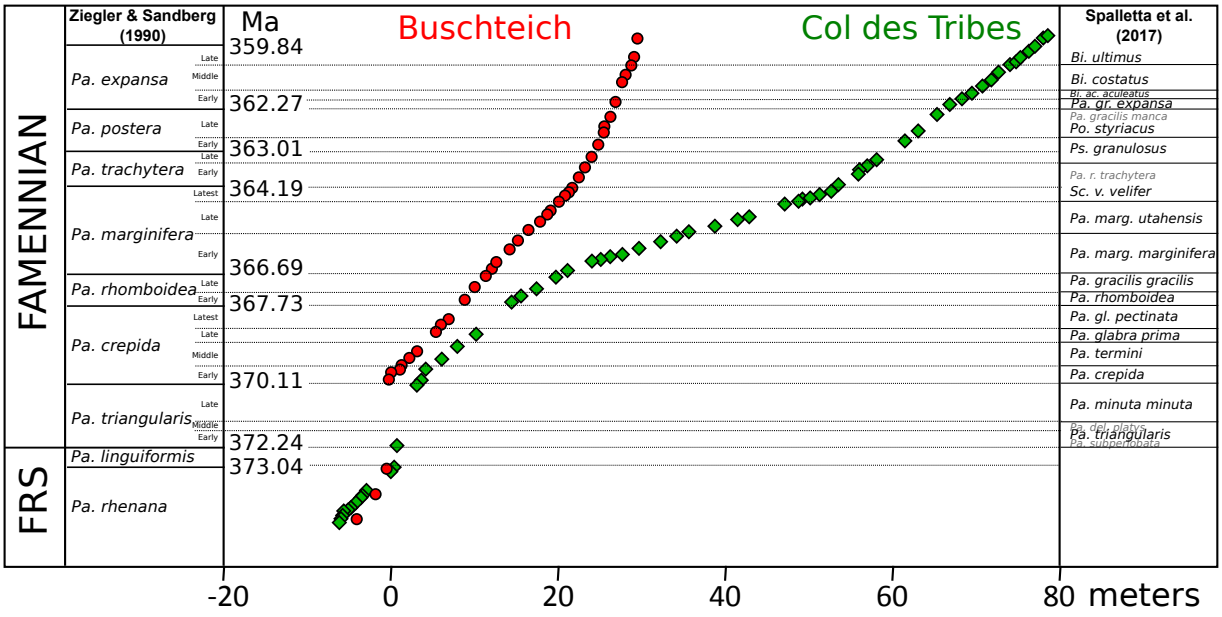
FAMENNIAN
FRS
Ziegler & Sandberg (1990)
Pa. expansa
Pa. postera
Pa. trachytera
Pa. marginifera
Pa. rhomboidea
Pa. crepida
Pa. triangularis
Pa. linguiformis
Pa. rhenana
Late
Middle
Early
Latest
Ma
359.84
362.27
363.01
364.19
366.69
367.73
370.11
372.24
373.04
Buschteich
Col des Tribes
Spalletta et al. (2017)
Bi. ultimus
Bi. costatus
Bi. ac. aculeatus
Pa. gr. expansa
Pa. gracilis manca
Po. styriacus
Ps. granulosus
Pa. r. trachytera
Sc. v. velifer
Pa. marg. utahensis
Pa. marg. marginifera
Pa. gracilis gracilis
Pa. rhomboidea
Pa. gl. pectinata
Pa. glabra prima
Pa. termini
Pa. crepida
Pa. minuta minuta
Pa. del. platys
Pa. triangularis
Pa. subperlobata
-20
0
20
40
60
80
meters

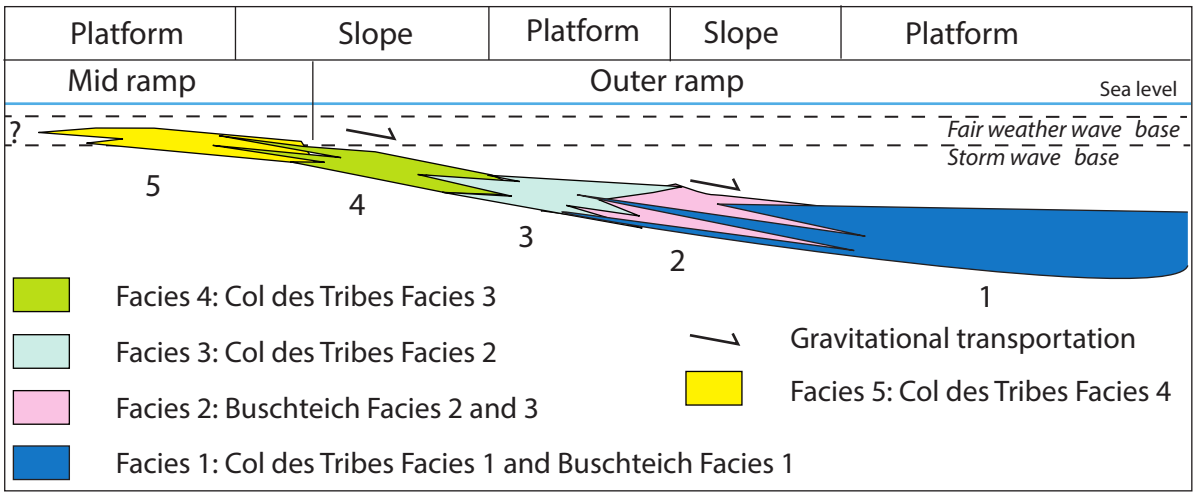
Platform
Slope
Platform
Slope
Platform
Mid ramp
Outer ramp
Sea level
?
Fair weather wave base
Storm wave base
5
4
3
2
1
Facies 4: Col des Tribes Facies 3
Facies 3: Col des Tribes Facies 2
Facies 2: Buschteich Facies 2 and 3
Facies 1: Col des Tribes Facies 1 and Buschteich Facies 1
Gravitational transportation
Facies 5: Col des Tribes Facies 4

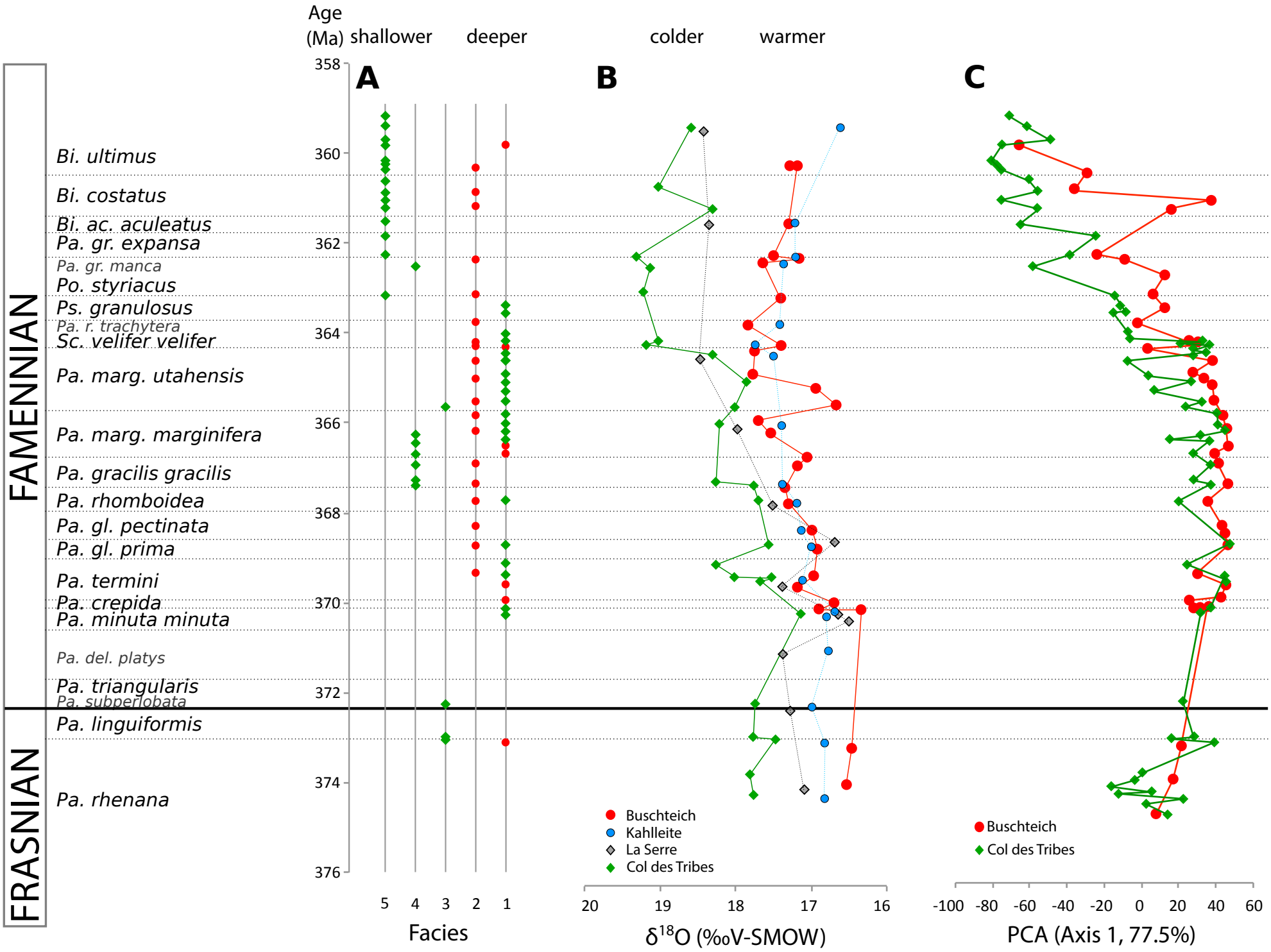
Age
(Ma)
shallower
deeper
colder
warmer
A
B
C
358
360
362
364
366
368
370
372
374
376
FAMENNIAN
FRASNIAN
Bi. ultimus
Bi. costatus
Bi. ac. aculeatus
Pa. gr. expansa
Pa. gr. manca
Po. styriacus
Ps. granulosus
Pa. r. trachytera
Sc. velifer velifer
Pa. marg. utahensis
Pa. marg. marginifera
Pa. gracilis gracilis
Pa. rhomboidea
Pa. gl. pectinata
Pa. gl. prima
Pa. termini
Pa. crepida
Pa. minuta minuta
Pa. del. platys
Pa. triangularis
Pa. subperlobata
Pa. linguiformis
Pa. rhenana
5 4 3 2 1
Facies
Buschteich
Kahlleite
La Serre
Col des Tribes
20 19 18 17 16
δ18O (‰V-SMOW)
Buschteich
Col des Tribes
-100 -80 -60 -40 -20 0 20 40 60
PCA (Axis 1, 77.5%)

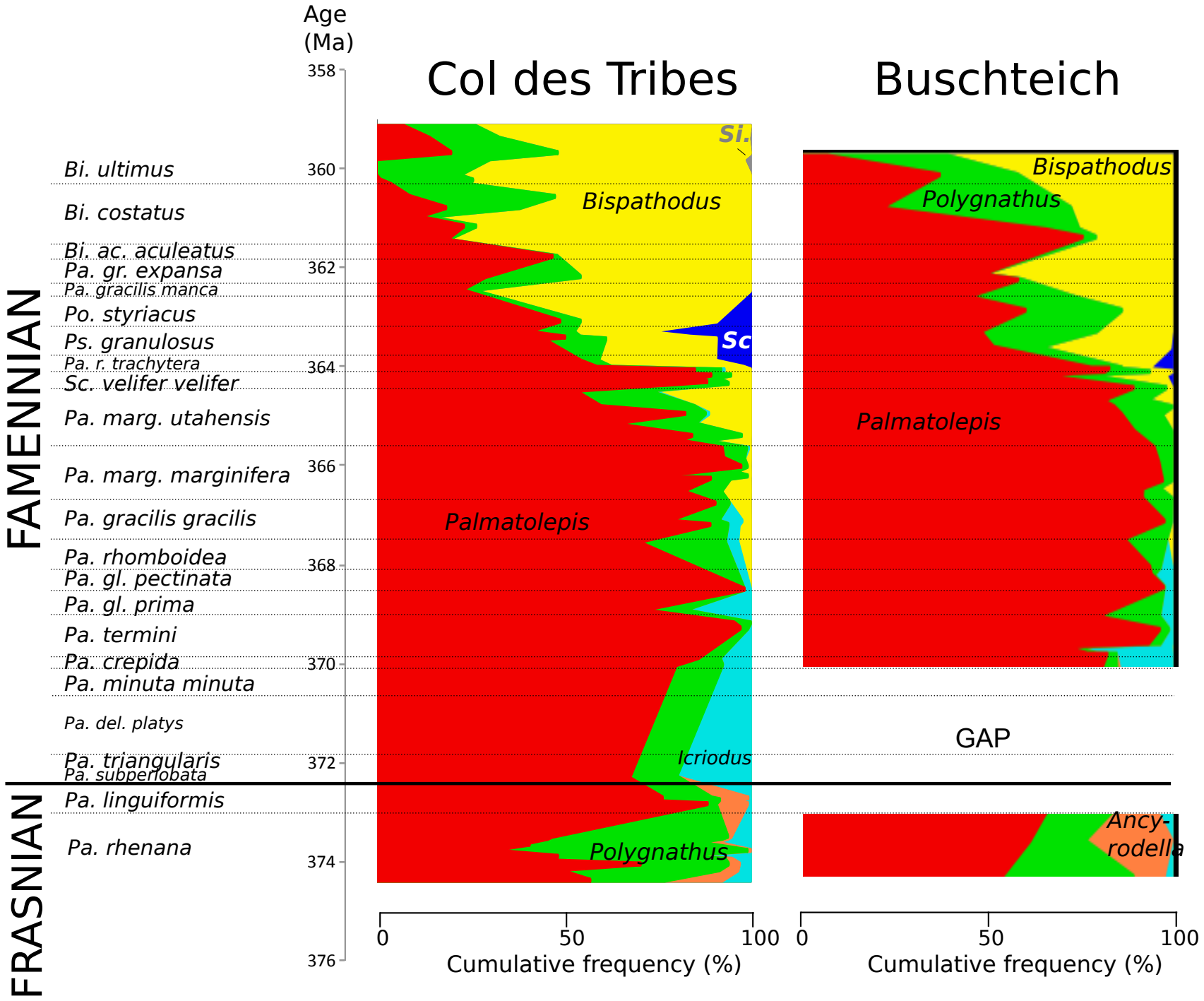
Age
(Ma)
358
360
362
364
366
368
370
372
374
376
Col des Tribes
Buschteich
FAMENNIAN
FRASNIAN
Bi. ultimus
Bi. costatus
Bi. ac. aculeatus
Pa. gr. expansa
Pa. gracilis manca
Po. styriacus
Ps. granulosus
Pa. r. trachytera
Sc. velifer velifer
Pa. marg. utahensis
Pa. marg. marginifera
Pa. gracilis gracilis
Pa. rhomboidea
Pa. gl. pectinata
Pa. gl. prima
Pa. termini
Pa. crepida
Pa. minuta minuta
Pa. del. platys
Pa. triangularis
Pa. subperlobata
Pa. linguiformis
Pa. rhenana
Si.
Bispathodus
Sc
Palmatolepis
Icriodus
Polygnathus
Bispathodus
Polygnathus
Palmatolepis
GAP
Ancy-
rodella
0
50
100
Cumulative frequency (%)
0
50
100
Cumulative frequency (%)

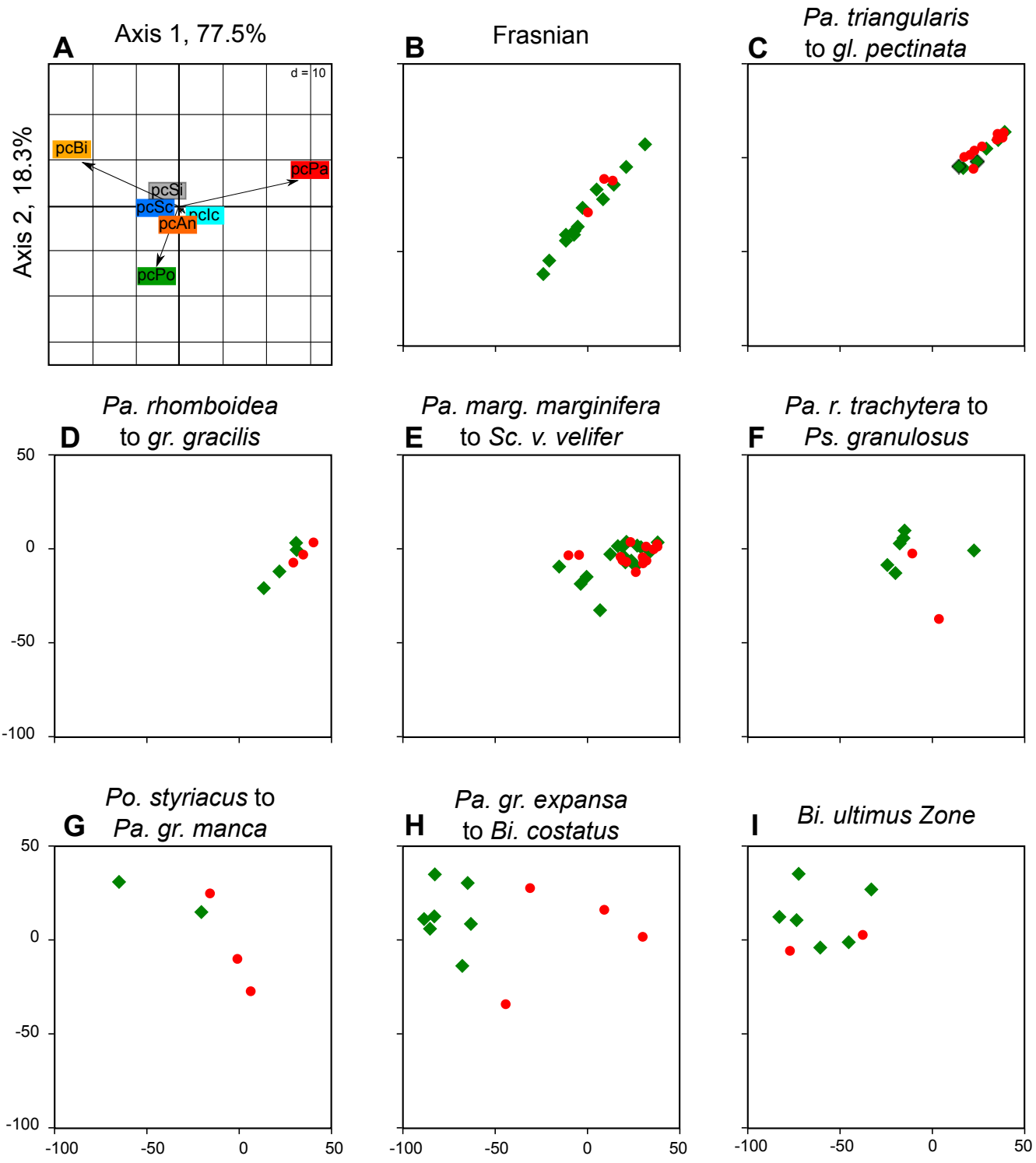
A
Axis 1, 77.5%
Axis 2, 18.3%
d = 10
pcBi
pcPa
pcSi
pcSc
pcIc
pcAn
pcPo
B
Frasnian
C
Pa. triangularis
to gl. pectinata
D
Pa. rhomboidea
to gr. gracilis
E
Pa. marg. marginifera
to Sc. v. velifer
F
Pa. r. trachytera to
Ps. granulosus
G
Po. styriacus to
Pa. gr. manca
H
Pa. gr. expansa
to Bi. costatus
I
Bi. ultimus Zone
50
0
-50
-100
-100
-50
0
50

Table 1. Facies and environmental settings for the Col des Tribes and the Buschteich sections

FACIES	DIAGNOSTIC FEATURES	SEDIMENTARY FEATURES	STRATAL PATTERN	BIOCLASTS	DEPOSITIONAL SETTING	Girard et al. *2014 (CT) **2017 (BU)
Facies 1 : pelagic mudstone	Structureless lime mudstone with few bioclasts (2 – 10%)		Well stratified, dms thick	Pelagic ostracods and bivalves, goniatites, radiolarians, rare benthic ostracods, trilobites and crinoids	Outer ramp	Facies 1 at CT and BU
Facies 2: fine-grained turbidites	Laminated wackestone with pelagic fauna and scarce hardparts of benthic organisms	Mm to cm scale thick graded bedding, erosional surfaces at bottom	dm thick beds	Pelagic ostracods and bivalves, radiolarians, some transported benthic ostracods, blind trilobites brachiopods and crinoids	Distal turbidites in outer ramp interbedded within F1	Facies 2 and 3 at BU
Facies 3: pelagic wackestone	Structureless wackestone dominated by pelagic fauna and with 5 % benthic organisms	Pseunodular structure	cm to dm thick beds	Pelagic bivalves and ostracods, diversified cephalopods, radiolarians, crinoids, benthic ostracods and trilobites	Outer ramp, shallower than F1 and F2	Facies 2 at CT
Facies 4: cephalopod wackestone to floatstone (griottes)	Reddish nodular to wavy laminated wackestone to floatstone with abundant goniatites	cm sized lime nodules coated by argillaceous and iron hydroxydes, intraformational breccias, rotated geopetal structures	Cm to dm thick beds	Goniatites, pelagic ostracods and bivalves, trilobites, brachiopods, crinoids and foraminifers	Slope in the upper outer ramp	Facies 3 at CT
Facies 5: wackestone with diversified fauna	Structureless to pseudonodular well stratified wackestone with pelagic and benthic organisms	Pseudonodular structure with cm to dm thick beds	cm to dm thick beds	Pelagic ostracods and abundant goniatites, trilobites, crinoids, brachiopods, gastropods, bivalves, foraminifers	Mid ramp	Facies 4 at CT

Table 2. Relationship between oxygen isotopes, microfacies, and conodont assemblages.

		CT+BU			CT			BU		
		n	R	p	n	R	p	n	R	p
$\delta^{18}O$	Facies	41	0.5023	**0.0008**	22	0.4107	0.0576	19	0.3149	0.1891
Conodont PC1	$\delta^{18}O$	51	-0.5304	**6.2e-5**	25	-0.5665	**0.0031**	26	-0.3039	0.1312
Conodont PC1	Facies	78	-0.6576	**6.1e-11**	52	-0.7058	**5.1e-09**	26	0.1799	0.3791
$\delta^{18}O$	Age	51	-0.5150	**0.0001**	25	-0.7532	**1.388e-05**	26	-0.7018	**6.455e-05**

Correlations between two variables using the Pearson's product-moment correlation, coefficient of correlation (R) and probability (p) are given. Analyses were performed for CT and BU combined, and CT and BU alone. Significant correlations marked in bold ($p < 0.05$). Age is estimated based on the age model.

Table 3. Analyses of variance on oxygen isotopes and conodont proportions.

			CT+ BU			CT			BU		
	Dependent variable	Independent variable	n	Pve	p	n	Pve	p	n	Pve	p
(1)	$\delta^{18}O$	Age	51	30.5%	**1.83E-09**						
		Section		47.0%	**4.06E-12**						
		Age * Section		0.4%	0.375						
(2)	Conodont PC1	$\delta^{18}O$	41	6.1%	**0.0311**	22	9.0%	**0.0316**	19	11.2%	0.175
		Facies		22.3%	**0.0001**		33.6%	**0.0003**		0.5%	0.769

Two models were considered. (1) A model considered $\delta^{18}O$ as dependent variable, and age, section, and interaction (age * section) as effects. (2) A model considered PC1 based on conodont proportions in the assemblages as the dependent variable. The effects tested were δ $\delta^{18}O$ and facies score. Percentage of variance explained (pve) and probability (p) are given. Significant correlations marked in bold ($p < 0.05$).